



ELASTIC WAVE MOTIONS IN AN AXIALLY STRAINED, INFINITELY LONG ROTATING TIMOSHENKO SHAFT

B. KANG AND C. A. TAN

Department of Mechanical Engineering, Wayne State University, Detroit, MI 48202, U.S.A.

(Received 19 May 1997, and in final form 8 January 1998)

In this paper, transverse waves propagating in an infinitely long, rotating Timoshenko shaft subjected to axial forces are studied. The model includes the contributions of axial deformation to the transverse vibration of the rotating shaft. Four different types of wave motions, two cut-off frequencies and frequency spectra are defined and discussed. The effects of rotation speed, axial force and axial deformation on the frequency spectra, phase velocity and group velocity are examined. It is found that the wave motions are generally independent of the rotation speed and the axial load significantly affects the wave motions at small real wavenumbers.

© 1998 Academic Press Limited

1. INTRODUCTION

Rotating flexible shafts are one of the most commonly employed mechanical elements for power transmission in industrial machines such as gas turbines, internal combustion engines and turbogenerators. Recent demands on the performance of these machine elements at high speeds and the application of lighter components require more reliable, failure-safe elements and the use of more accurate models for analysis. Three beam theories, the Euler–Bernoulli, Rayleigh and Timoshenko models, are commonly employed to examine the transverse vibrations of rotating flexible shafts. In the Timoshenko model, both the rotary inertia and shear deformation effects are included. As more accurate analyses are required, it is recognized that the Timoshenko theory is needed to accurately predict the frequencies and vibration modes of stubby beams [1] used in such applications as automotive crank-shaft mechanisms.

Numerous studies of the vibrations of rotating shafts employing the three beam theories have been presented and well documented [2–4]. A consistent modelling of rotating Timoshenko shafts subjected to axial loads by applying a finite strain beam theory and Hamilton's principle was proposed in reference [5]. Other studies focus on the development of techniques to investigate the dynamic response and vibrations of different rotating shaft models. Katz *et al.* [6] introduced a finite integral transform method for evaluating the transient response of rotating Rayleigh and Timoshenko shafts. An alternative approach to the same problem was presented by Han and Zu [7]. They used a modal analysis technique and extended the work of reference [6] to the response analysis of Timoshenko shafts with general boundary conditions. Recently, Tan and Kuang [8] obtained exact, closed-form solutions for the free and forced responses of a stepped, rotating Timoshenko shaft by the distributed transfer function method and a generalized displacement formulation.

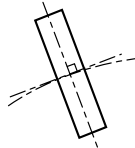
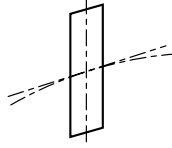
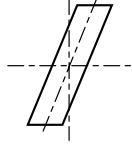
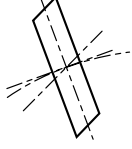
In addition to being a more refined theory, the Timoshenko beam model has two frequency spectra [9, 10]. The first spectrum corresponds primarily to the classical beam bending, while the second spectrum is a result of including shear deformation in the model. Abbas and Thomas [9] argued that the second frequency spectrum could only be found in the case of a hinged–hinged beam. However, Bhashyam and Prathap [10] applied a linear finite element method to show that this frequency spectrum also existed in other cases of boundary conditions. Three different component or constituent modes of vibration, the Euler–Bernoulli, simple shear and pure shear modes (hereafter denoted by E-B, SS and PS, respectively) were defined to explain the vibration of a Timoshenko beam at various frequencies [9, 10]. Table 1 summarizes the characteristics of each constituent mode in comparison to the Timoshenko model. The vibration of a Timoshenko beam is considered to be a combination of these constituent modes.

The vibrations of simple elastic structures such as strings, beams, and plates can be described in terms of waves propagating and attenuating in waveguides. The subject of wave motions has also been studied extensively in the fields of acoustics in fluids and solids [11–13]. One of the advantages of applying the wave propagation technique to study the mechanical vibrations of structures is its ability to provide a compact and systematic methodology to analyse complex structures such as trusses, aircraft panels with periodic supports, and beams on multiple supports [14]. Using the phase-closure principle, Mead [15] presented a method to calculate the natural frequencies of Euler–Bernoulli beam models. By employing concepts of wave reflection and transmission, Mace [16] applied the wave propagation approach to obtain the system natural frequencies of Euler–Bernoulli beam models including waves of both propagating and near-field types. Despite the usefulness of the wave propagation technique, it has seldom been applied to the problem of a rotating flexible shaft, except in reference [17] where the effects of the rotation speed on the frequency spectra and group velocity are examined for an infinitely long, rotating Timoshenko beam.

This is a two-part study on the elastic wave motions in rotating Timoshenko shafts subjected to axial loads. The purpose of this paper is to investigate the general characteristics of the wave propagation by considering the infinitely long beam problem. A sequel paper [18] examines the wave reflection and transmission under arbitrary geometric discontinuities, support and boundary conditions. This manuscript is organized

TABLE 1

Comparison of various constituent beam models with the Timoshenko beam theory

	Euler–Bernoulli (E–B)	Simple shear (SS)	Pure shear (PS)	Timoshenko
Transverse displacement	Yes	Yes	No	Yes
Rotation of cross-section	Yes	No	Yes	Yes
Shearing motion	No	Yes	Yes	Yes
Schematic of vibration of an infinitesimal element				

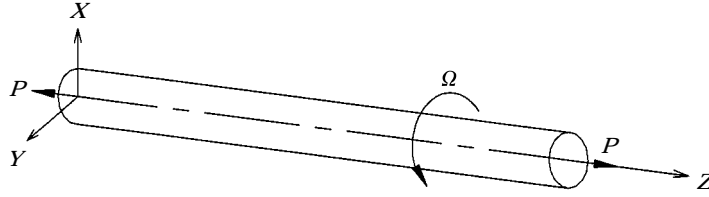


Figure 1. A rotating Timoshenko shaft model subject to axial loads.

as follows. The equations of motion and normalization are described in section 2. In section 3, the frequency and cut-off frequencies are derived. General wave solutions and the effects of rotation speed and axial load on the frequency spectra, phase velocity and group velocity are then examined and discussed.

2. EQUATIONS OF MOTION

Consider a rotating Timoshenko shaft subject to axial loads, as shown in Figure 1. By Hamilton's Principle and a finite strain beam theory [5] which is geometrically exact and capable of accounting for large shearing strains, axial strain, curvature, and twist, the linearized equation governing the flexural motion of the rotating shaft is

$$\begin{aligned} & \frac{EI}{\rho A_s} \frac{\partial^4 U}{\partial Z^4} - \left(\frac{EI}{KA_s G} + \frac{J}{\rho A_s} \right) \frac{\partial^4 U}{\partial Z^2 \partial T^2} + i \frac{J_p \Omega}{\rho A_s} \frac{\partial^3 U}{\partial Z^2 \partial T} + \frac{\partial^2 U}{\partial T^2} - i \frac{J_p \Omega}{KA_s G} \frac{\partial^3 U}{\partial T^3} + \frac{J}{KA_s G} \frac{\partial^4 U}{\partial T^4} \\ & - \frac{P}{\rho A_s} \left(1 - \frac{P}{KA_s G} \right) \frac{\partial^2 U}{\partial Z^2} - \frac{P}{KA_s G} \frac{\partial^2 U}{\partial T^2} - \frac{P^2}{KA_s \cdot EA_s} \frac{\partial^2 U}{\partial Z^2} \\ & + \left[\frac{2P}{EA_s} - \frac{P^2}{EA_s \cdot KA_s G} + \frac{P^2}{(EA_s)^2} \right] \frac{\partial^2 U}{\partial T^2} = 0, \end{aligned} \quad (1)$$

where U is the transverse displacement in the complex notation

$$U = U_x + iU_y, \quad (2)$$

and U_x and U_y denote the displacements in the X and Y directions, respectively with respect to a fixed reference frame, E the Young's modulus, I the lateral area moment of inertia of the cross-section, ρ the mass density, A_s the area of the cross-section, K the Timoshenko shear coefficient, G the shear modulus, J the lateral mass moment of inertia of the cross-section per unit length, J_p the polar mass moment of inertia of the cross-section per unit length, and Ω the constant angular velocity of the shaft. In this model, damping and axial deformation due to inertia are neglected. Note that the last four terms of equation (1) involve the axial stiffness EA_s . These additional linear terms are associated with axial deformations and take into account the effects of axial extension on the transverse displacements of the axially loaded Timoshenko shaft model. As will be shown, these effects become more pronounced as the magnitude of the axial load increases and as the wavelength becomes small. The significance of these terms is also discussed in reference [5].

Introduce the following non-dimensional variables and parameters:

$$u = \frac{U}{a_0}, \quad z = \frac{Z}{a_0}, \quad t = \frac{T}{T_0}, \quad T_0 = \sqrt{\frac{\rho a_0^2}{KG}}; \quad (3a)$$

$$\alpha = \frac{KG}{E}, \quad \beta = \frac{\rho a_0^2}{ET_0} \Omega = \frac{\rho a_0 c_s}{E} \Omega, \quad \varepsilon = \frac{P}{EA_s}, \quad (3b)$$

where a_0 is the diameter of shaft and T_0 is a characteristic time constant, $c_s = \sqrt{KG/\rho}$ is the *shear wave velocity*, and ε is the axial strain. Employing $2J = J_p$ in equation (1) for circular beams yields the normalized equation of motion

$$\begin{aligned} \frac{\partial^4 u}{\partial z^4} - (1 + \alpha) \frac{\partial^4 u}{\partial z^2 \partial t^2} + 2i\beta \frac{\partial^3 u}{\partial z^2 \partial t} - 2i\beta \frac{\partial^3 u}{\partial t^3} + \alpha \frac{\partial^4 u}{\partial t^4} - 16\varepsilon \left(1 + \varepsilon - \frac{\varepsilon}{\alpha}\right) \frac{\partial^2 u}{\partial z^2} \\ + 16\alpha(1 + \varepsilon) \left(1 + \varepsilon - \frac{\varepsilon}{\alpha}\right) \frac{\partial^2 u}{\partial t^2} = 0. \end{aligned} \quad (4)$$

The equation of motion governing the rotation (due to bending) of the cross-section of an infinitesimal element of the shaft model can be obtained in the same manner as

$$\begin{aligned} \frac{\partial^4 \Psi}{\partial z^4} - (1 + \alpha) \frac{\partial^4 \Psi}{\partial z^2 \partial t^2} + 2i\beta \frac{\partial^3 \Psi}{\partial z^2 \partial t} - 2i\beta \frac{\partial^3 \Psi}{\partial t^3} + \alpha \frac{\partial^4 \Psi}{\partial t^4} - 16\varepsilon \left(1 + \varepsilon - \frac{\varepsilon}{\alpha}\right) \frac{\partial^2 \Psi}{\partial z^2} \\ + 16\alpha(1 + \varepsilon) \left(1 + \varepsilon - \frac{\varepsilon}{\alpha}\right) \frac{\partial^2 \Psi}{\partial t^2} = 0, \end{aligned} \quad (5)$$

where Ψ is the measurement of the slope of the cross-section due to bending in the complex notation. The transverse shearing deformation is measured by the difference $i(\partial u(z, t)/\partial z) - \Psi(z, t)$.

3. PROPAGATION OF HARMONIC WAVES

Since a vibrating beam is a dispersive medium for transverse waves, the phase velocity c is not constant. Hence, the simple wave solution of the form $f(z \pm ct)$ with constant phase velocity c does not satisfy equations (4) and (5). In a complex wave with several frequency components, each component travels at a different speed, thereby distorting the shape of the wave. To study the wave propagation in this Timoshenko shaft model, it is necessary to first determine the conditions under which the following wave solutions,

$$u(z, t) = C_u e^{i(\bar{\gamma}z + \bar{\omega}t)}, \quad \Psi(z, t) = C_\Psi e^{i(\bar{\gamma}z + \bar{\omega}t)}, \quad (6a, b)$$

satisfy the equations of motion, where $\bar{\gamma}$ and $\bar{\omega}$ are the non-dimensionalized wavenumber and frequency, respectively, and are defined as

$$\bar{\gamma} = \gamma a_0, \quad \bar{\omega} = \omega a_0 / c_s. \quad (6c)$$

Note that from the kinematic relationship

$$\frac{\partial^2 u}{\partial t^2} = \frac{\partial^2 u}{\partial z^2} + i \left(1 + \varepsilon - \frac{\varepsilon}{\alpha}\right) \frac{\partial \Psi}{\partial z}, \quad (7a)$$

the wave amplitudes C_u and C_ψ , are not independent, and their amplitude ratio is

$$\frac{C_\psi}{C_u} = \frac{\bar{\omega}^2 - \bar{\gamma}^2}{\bar{\gamma}(1 + \varepsilon - \varepsilon/\alpha)}. \tag{7b}$$

The propagation direction has arbitrarily been selected in equations (6a, b).

Substituting the harmonic wave solution (6a) into equation (4) leads to the frequency equation

$$\begin{aligned} \alpha\bar{\omega}^4 - 2\beta\bar{\omega}^3 - \left[(1 + \alpha)\bar{\gamma}^2 + 16\alpha(1 + \varepsilon)\left(1 + \varepsilon - \frac{\varepsilon}{\alpha}\right) \right] \bar{\omega}^2 + 2\beta\bar{\gamma}^2\bar{\omega} \\ + \bar{\gamma}^2 \left[\bar{\gamma}^2 + 16\varepsilon\left(1 + \varepsilon - \frac{\varepsilon}{\alpha}\right) \right] = 0, \end{aligned} \tag{8}$$

or in terms of the wavenumber $\bar{\gamma}$,

$$\bar{\gamma}^4 - A\bar{\gamma}^2 + B = 0, \tag{9a}$$

where,

$$\begin{aligned} A &= (1 + \alpha)\bar{\omega}^2 - 2\beta\bar{\omega} - 16\varepsilon(1 + \varepsilon - \varepsilon/\alpha), \\ B &= \bar{\omega}^2[\alpha\bar{\omega}^2 - 2\beta\bar{\omega} - 16\alpha(1 + \varepsilon)(1 + \varepsilon - \varepsilon/\alpha)]. \end{aligned} \tag{9b, c}$$

Taking the long-wavelength limit ($\bar{\gamma} \rightarrow 0$) of equation (9a) leads to

$$B = 0 \quad \text{or} \quad \bar{\omega}^2 \left[\alpha\bar{\omega}^2 - 2\beta\bar{\omega} - 16\alpha(1 + \varepsilon)\left(1 + \varepsilon - \frac{\varepsilon}{\alpha}\right) \right] = 0. \tag{10}$$

Solving for the roots of the above equation gives

$$\bar{\omega}_c^I = 0 \quad \text{and} \quad \bar{\omega}_c^{II} = \frac{\beta}{\alpha} \pm \sqrt{\left(\frac{\beta}{\alpha}\right)^2 + 16(1 + \varepsilon)\left(1 + \varepsilon - \frac{\varepsilon}{\alpha}\right)}, \tag{11a, b}$$

where $\bar{\omega}_c$ denotes the *cut-off frequency* and the superscripts I and II denote the corresponding wave propagation modes. Note that the Euler–Bernoulli beam model has only one cut-off frequency $\bar{\omega}_c = 0$ for the flexural mode. But the Timoshenko shaft model has two cut-off frequencies, $\bar{\omega}_c^I$ and $\bar{\omega}_c^{II}$, leading to the first frequency spectrum (hereafter denoted by S^I) and the second frequency spectrum (S^{II}), respectively. The vibrating motion of the rotating shaft corresponding to each cut-off frequency can be identified by examining the amplitude ratio between the two wave solutions $u(z, t)$ and $\Psi(z, t)$, see equations (7b). When $\bar{\omega} \rightarrow \bar{\omega}_c^I$, equation (7b) reveals that $C_u \neq 0$ and $C_\psi = 0$, so that the shaft experiences a rigid body motion with $\Psi = 0$ (i.e., no rotation of the cross-section of the infinitesimal element). When $\bar{\omega} \rightarrow \bar{\omega}_c^{II}$, equation (7b) reveals that $C_u = 0$ and $C_\psi \neq 0$, implying a shearing motion wherein all cross-sections of the shaft rotate back and forth in unison. Hence, at $\bar{\omega}_c^{II}$, the vibrating shaft experiences no transverse displacement, that is

$$u(z, t) = 0 \quad \text{and} \quad \Psi(z, t) = C_\psi e^{i\bar{\omega}_c^{II}t}. \tag{12}$$

This solution corresponds to the pure shear mode [10] of the rotating Timoshenko shaft model.

4. FREQUENCY SPACES AND GENERAL WAVE SOLUTIONS

Before presenting numerical results for the frequency spectra of the rotating Timoshenko shaft model, the frequency equation is further analysed by examining the algebraic relations between the wavenumber and the coefficients A and B in equations (9a). This analysis leads to a better understanding of the relationships between wavenumbers and frequencies, and criteria for determining the proper wave solutions under a given set of physical parameters. The four roots of equation (9a) are

$$\bar{\gamma} = \pm \frac{1}{\sqrt{2}} (A \pm \sqrt{A^2 - 4B})^{1/2}. \quad (13)$$

For $\alpha > 0$ and $|\varepsilon| < 1$ (ε is the actual strain of an elastic solid), numerical results over a wide range of physical parameters show that the discriminant $A^2 - 4B$ is semi-positive definite for most engineering applications. Employing this fact and assuming that $\bar{\omega}$ is real, it can readily be shown that $\bar{\gamma}$ is either real or imaginary. The general wave solutions can then be classified into four cases as follows.

Case I ($A > 0$ and $B > 0$; all roots of equation (9a) are real)

$$u(z, t) = (C_1^+ e^{-\bar{\gamma}_1 z} + C_1^- e^{\bar{\gamma}_1 z} + C_2^+ e^{-\bar{\gamma}_2 z} + C_2^- e^{\bar{\gamma}_2 z}) e^{i\bar{\omega} t}, \quad (14a)$$

Case II ($A > 0$ and $B < 0$; two roots of equation (9a) are real and two are imaginary)

$$u(z, t) = (C_1^+ e^{-\bar{T}_1 z} + C_1^- e^{\bar{T}_1 z} + C_2^+ e^{-\bar{T}_2 z} + C_2^- e^{\bar{T}_2 z}) e^{i\bar{\omega} t}, \quad (14b)$$

Case III ($A < 0$ and $B > 0$; all roots of equation (9a) are imaginary)

$$u(z, t) = (C_1^+ e^{-\bar{\gamma}_1 z} + C_1^- e^{\bar{\gamma}_1 z} + C_2^+ e^{-\bar{\gamma}_2 z} + C_2^- e^{\bar{\gamma}_2 z}) e^{i\bar{\omega} t}, \quad (14c)$$

Case IV ($A < 0$ and $B < 0$; two roots of equation (9a) are real and two are imaginary)

$$u(z, t) = (C_1^+ e^{-\bar{T}_1 z} + C_1^- e^{\bar{T}_1 z} + C_2^+ e^{-\bar{T}_2 z} + C_2^- e^{\bar{T}_2 z}) e^{i\bar{\omega} t}, \quad (14d)$$

where

$$\bar{\gamma}_1 = \frac{1}{\sqrt{2}} (|A| + \sqrt{A^2 - 4|B|})^{1/2}, \quad \bar{\gamma}_2 = \frac{1}{\sqrt{2}} (|A| - \sqrt{A^2 - 4|B|})^{1/2}, \quad (14e, f)$$

$$\bar{T}_1 = \frac{1}{\sqrt{2}} (\sqrt{A^2 + 4|B|} + |A|)^{1/2}, \quad \bar{T}_2 = \frac{1}{\sqrt{2}} (\sqrt{A^2 + 4|B|} - |A|)^{1/2}, \quad (14g, h)$$

and the coefficients C^+ and C^- denote positive-travelling and negative-travelling waves from the origin of disturbance along the Timoshenko shaft, respectively. In all the figures presented in this paper, system parameters adopted from Katz *et al.* [6] are used: $a_0 = 0.0955$ m, $\rho = 7700$ kg/m³, $E = 207 \times 10^9$ N/m², $G = 77.7 \times 10^9$ N/m², and $K = 0.9$. Unless otherwise stated, the overbar for non-dimensional variables is dropped hereafter for convenience.

Figures 2 and 3 plot the frequency spaces demarcated by the cut-off frequencies ($B = 0$) and $A = 0$, as functions of β and ε . As shown in the figures, the wave solution of *Case III* does not exist in the real frequency space since this solution dictates that none of the wave components can propagate. This case is of no interest in engineering applications. Therefore, in each demarcated region of the frequency spaces, one of the three wave solutions (*Cases I, II, and IV*) governs the wave motion. Figure 2 plots the frequency spaces corresponding to the general wave solutions for three different loading conditions as a function of the rotation speed. Figure 2(a) shows that in the presence of a compressive loading, the frequency for $A = 0$, $B < 0$ is complex, and it becomes real at a sufficiently

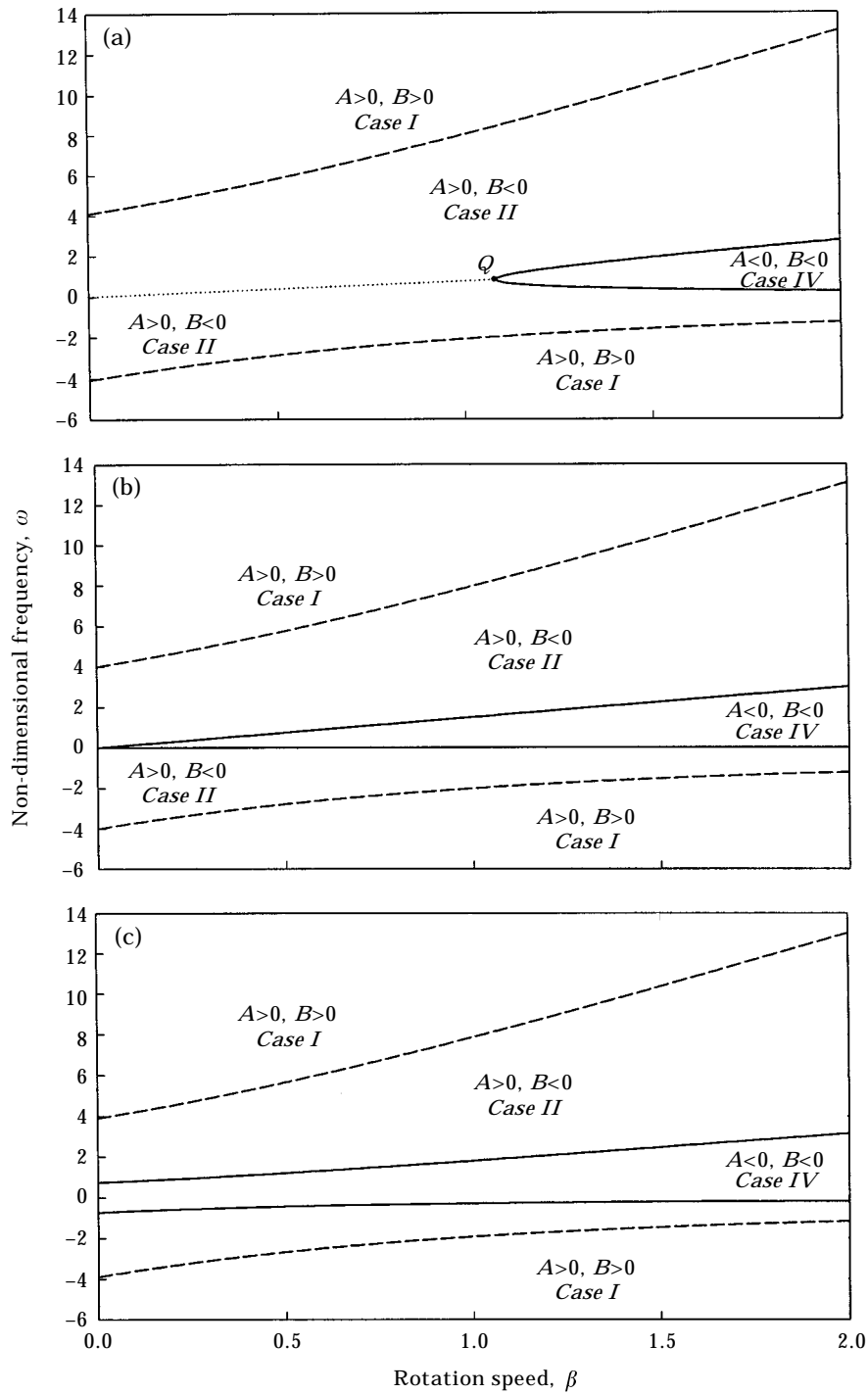


Figure 2. Frequency spaces demarcated by $A = 0$ (—) and non-zero cut-off frequencies $B = 0$ (---) as a function of rotation speed; $\alpha = 0.3378$. (a) $\varepsilon = -0.05$, (b) $\varepsilon = 0$, (c) $\varepsilon = 0.05$. Dotted curve (\cdots) indicates that ω is complex.

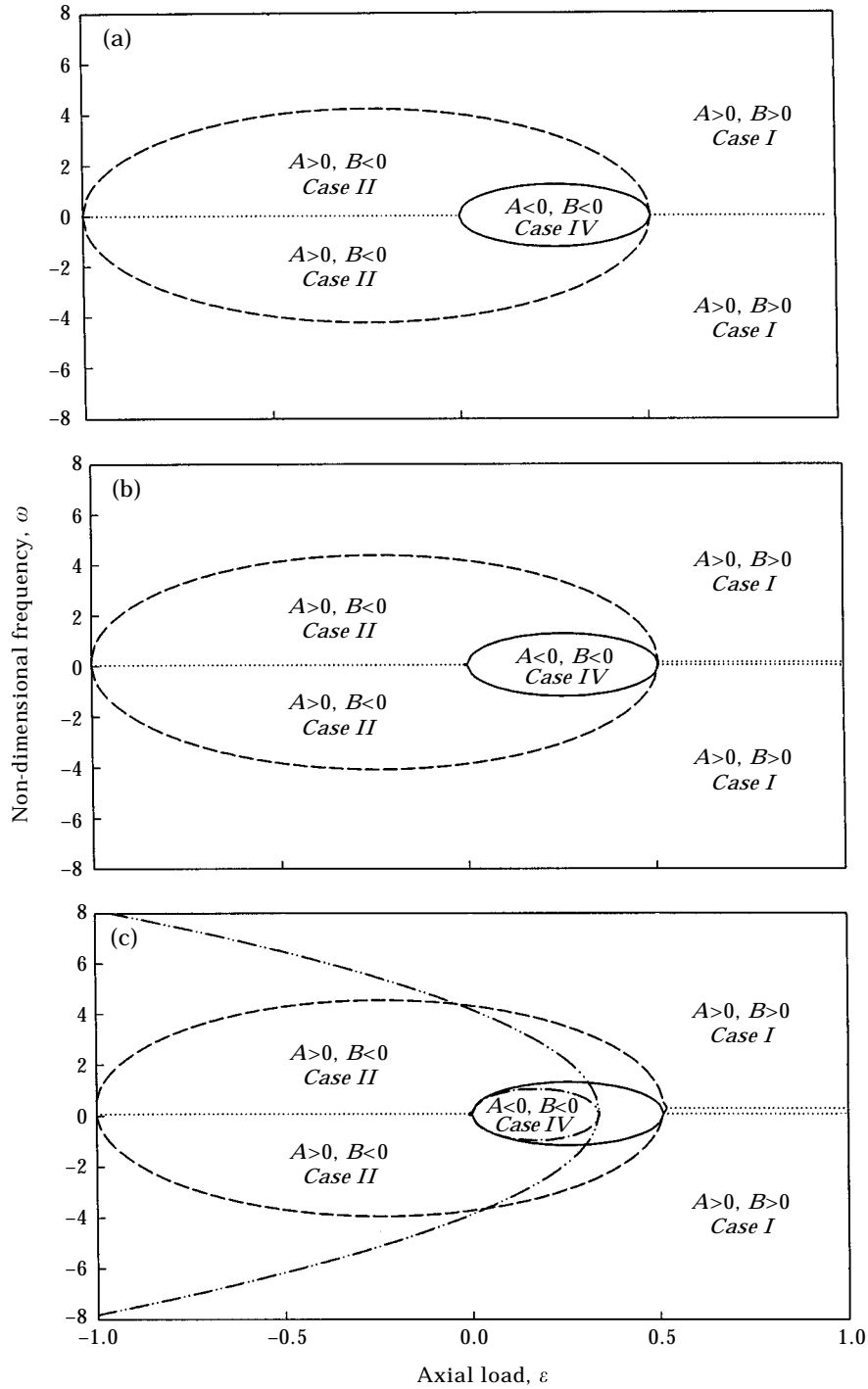


Figure 3. Frequency spaces demarcated by $A = 0$ (—) and non-zero cut-off frequencies $B = 0$ (---) as a function of axial load; $\alpha = 0.3378$. (a) $\beta = 0$, (b) $\beta = 0.05$, (c) $\beta = 0.1$. Also shown are $A = 0$ (- · - ·) and $B = 0$ (- · - ·) when effects of axial deformation are neglected. Dotted curves (· · · ·) indicate that ω is complex.

high rotation speed where the demarcation curve bifurcates (at point Q) and the gyroscopic effect dominates the effect of the axial loading. However, this high rotation speed is in general not attainable in practical engineering applications. Hence, in the range of practical operating rotation speeds, it can be concluded that *Case I* and *Case II* solutions govern the wave motions of a Timoshenko shaft subject to compressive loads. As in the case of Figure 2(a), Figures 3(a-c) also show that, when the rotating shaft model is subjected to compressive loads, only two wave solutions govern the entire frequency spaces for practical engineering applications. In Figures 3(a-c), the dot-dot-dashed demarcation curves show the differences when the shaft is modelled as axially inextensional. It is clearly seen that the demarcation curves are not closed in these cases. This means that the demarcation curves are still well defined as the compressive load increases beyond $\epsilon = -1$. These situations are physically unacceptable.

4.1. FREQUENCY SPECTRUM

The effects of the rotation speed on frequency and group velocity spectra have been examined in reference [17] for a shaft under no axial load. It is shown that, in the range of practical operating conditions, the rotation speed has little influence on the wave propagation characteristics. In this study, the effects of rotation speed and axial load on the wave motions are investigated for a shaft model including the contributions of the axial deformation.

Figure 4 plots the real frequency spectra against the real and imaginary parts of γ for three rotation speeds and $\epsilon = 0$. It is seen that the Timoshenko shaft model has two distinct frequency spectra. Following references [9, 10], the first frequency spectrum S' (lower branch) can be identified as the improved frequency spectrum of the simple Euler-Bernoulli shaft model. The vibration of the shaft is a coupled E-B and SS mode, with the E-B mode dominating at low γ and the SS mode dominating at high γ . Below S' , none of the wave components can propagate. The second frequency spectrum S'' (upper

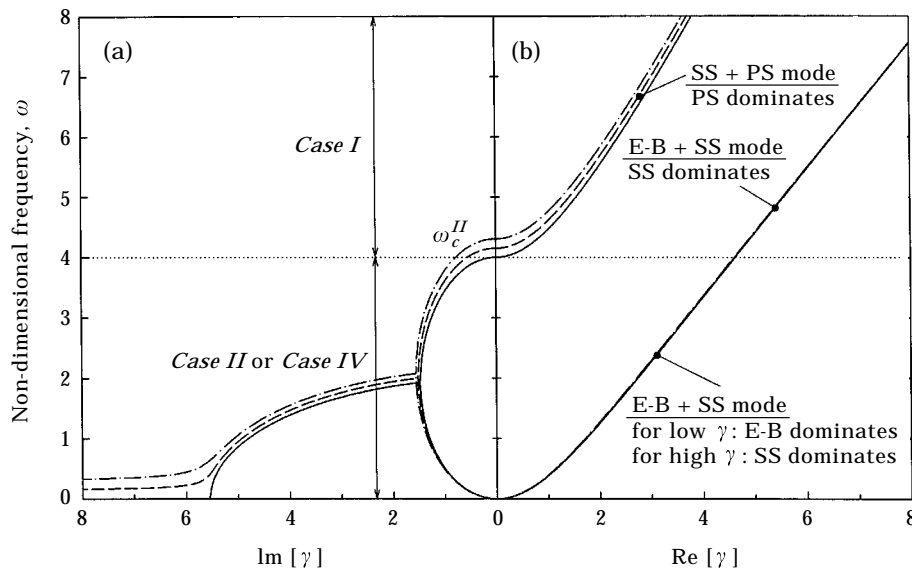


Figure 4. Non-dimensional real frequency spectra of an infinitely long Timoshenko shaft for three rotation speeds; $\alpha = 0.3378$ and $\epsilon = 0$; $\beta = 0$ (—), $\beta = 0.05$ (- - -), $\beta = 0.1$ (- · -); (a) as function of $\text{Im}[\gamma]$, (b) $\text{Re}[\gamma]$.

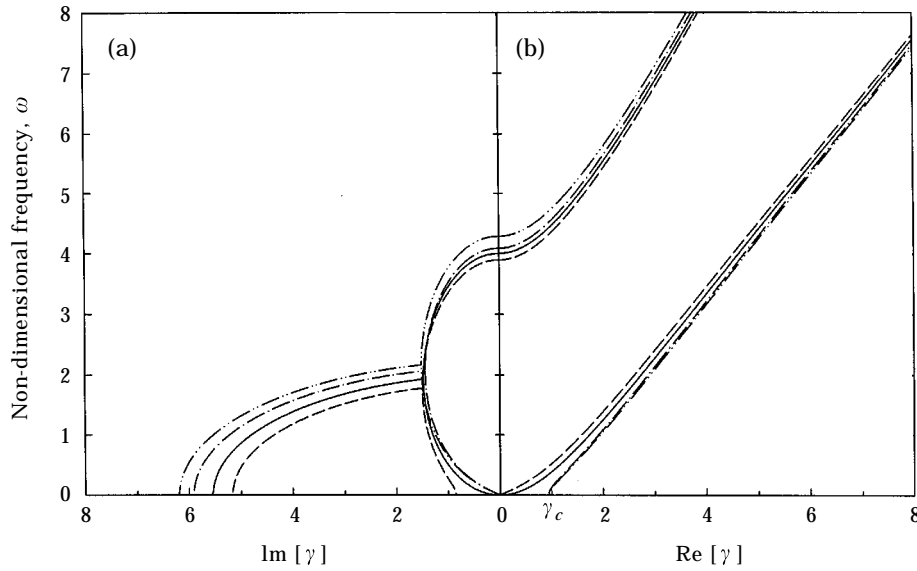


Figure 5. Non-dimensional real frequency spectra of an infinitely long Timoshenko shaft for three loading conditions; $\alpha = 0.3378$ and $\beta = 0$; $\varepsilon = 0$ (—), $\varepsilon = 0.05$ (---), $\varepsilon = -0.05$ (- · - ·), $\varepsilon = -0.05$ with effects of axial deformation neglected (- · · -); (a) as function of $\text{Im}[\gamma]$, (b) $\text{Re}[\gamma]$.

branch) represents a coupled SS and PS mode, with the PS mode dominating. From equations (14a–d), depending on the rotation speed and axial load, the vibration of the shaft below ω_c'' is governed by the wave solution of *Case II* or *IV*. While the shaft vibration above ω_c'' is governed by the wave solution of *Case I*. Note that for the wave solutions of *Cases II* and *IV*, imaginary wavenumbers also exist and these are plotted in Figure 4(a). Figure 4 is useful for determining the proper wave solutions of the finite shaft problem. Suppose the natural frequencies are estimated from some experimental data. The parameters A and B are first calculated to determine the type of wave solution. The corresponding wavenumbers are then obtained from Figure 4. Substituting these solutions into one of equation (14) and imposing the boundary conditions leads to solutions for the eigenfunctions of the finite rotating shaft. Note that only backward propagating wave solutions (C^- components) are plotted in Figure 4. A similar set of curves can be obtained for negative ω .

Figure 4 shows that the effects of the shaft rotation speed are more significant on S'' than S' . Indeed, S' is basically independent of β , even at very high rotation speeds ($\beta = 0.1$ is about 90 000 r.p.m.). In Figure 4(a), the spectrum S' increases with $\text{Im}[\gamma]$ (attenuating waves), while S'' decreases with $\text{Im}[\gamma]$ until the two frequency spectra coalesce at a certain wavenumber; e.g., at $\text{Im}[\gamma] = 1.48$ in the $\beta = 0$ case. For imaginary wavenumbers greater than this critical value, the two spectra are identical, and the frequencies are complex with diminishing real parts. Interpretation of complex frequency spectra in rotating Timoshenko shafts is not addressed here and will be examined in another paper. It is noted that, with increasing $\text{Im}[\gamma]$, the real part of the frequency vanishes (i.e., ω becomes imaginary) in the $\beta = 0$ case, but remains non-zero in the $\beta \neq 0$ cases. This implies that the rotation of the shaft causes an otherwise non-oscillatory temporal response to become oscillatory (with growing or decaying amplitudes depending on the sign of $\text{Im}[\omega]$).

Figure 5 plots the real frequency spectra versus the real and imaginary wavenumbers for three loading conditions and $\beta = 0$. Comparing Figure 5(b) with Figure 4(b), it is seen that the effects of the axial load on both frequency spectra are stronger than those of the rotation speed. The compressive load decreases S' and increases S'' . In other words, for a given frequency, the wavelengths of S' propagating waves are shortened while the wavelengths of S'' propagating waves are lengthened when the rotating shaft is being compressed. Application of a tensile load has the reverse effects. Note that, when a compressive load is applied to the shaft, there exists a critical wavenumber γ_c below which the frequency is imaginary (numerical results show that the frequency is positive imaginary). Hence, no S' wave can propagate in the range $0 < \gamma < \gamma_c$. The effects of the axial load on the attenuating waves are shown in Figure 5(a). For a given frequency and when the shaft is compressed, $\text{Im}[\gamma]$ decreases for S' waves and increases for S'' waves. Thus, in the presence of a compressive load, the rate of attenuation becomes smaller for S' waves. Again the tensile load has the reverse effects.

The dot-dot-dashed curves in Figure 5 are the results when the effects of axial deformation are neglected in the model. Only the case of compressive loading is shown. It is seen that the effects of the axial deformation are insignificant for the S' spectrum, while frequencies are increased (over-predicted) for the S'' spectrum. Numerical results show that this over-prediction increases with the axial strain. Therefore, the effects of axial deformation should be considered in wave propagation studies; this is discussed in reference [18] on the wave reflection and transmission in rotating Timoshenko shafts under general supports, discontinuities and boundaries.

4.2. DISPERSION CURVE AND GROUP VELOCITY

Applying the relationship $\omega = c\gamma$ to equation (8) gives the dispersion equation

$$(c^2 - 1)(\alpha c^2 - 1)\gamma^4 + 2\beta c(1 - c^2)\gamma^3 - 16\alpha\left(1 + \varepsilon - \frac{\varepsilon}{a}\right)\left[(1 + \varepsilon)c^2 - \frac{\varepsilon}{\alpha}\right]\gamma^2 = 0, \quad (15)$$

where c is the phase velocity. Vanishing of the first term in equation (15) gives the asymptotic behaviour ($\gamma \rightarrow \infty$) of the dispersion curves,

$$c_\infty^2 = 1 \quad \text{and} \quad c_\infty^2 = \frac{1}{\alpha}, \quad (16)$$

or expressed in terms of dimensional physical parameters (note that overbar for non-dimensional variables has been dropped for convenience),

$$c_\infty = \pm \sqrt{\frac{KG}{\rho}} = \pm c_s \quad \text{and} \quad c_\infty = \pm \sqrt{\frac{E}{\rho}} = \pm c_0, \quad (17)$$

where c_s is the shear velocity and c_0 is the wave velocity of a bar. Note that the asymptotic phase velocities c_∞ in equation (17) are independent of the rotation speed and the axial load. Hence, phase velocities are always bounded at large wavenumbers and there are two operative modes (corresponding to the S' and S'' spectra).

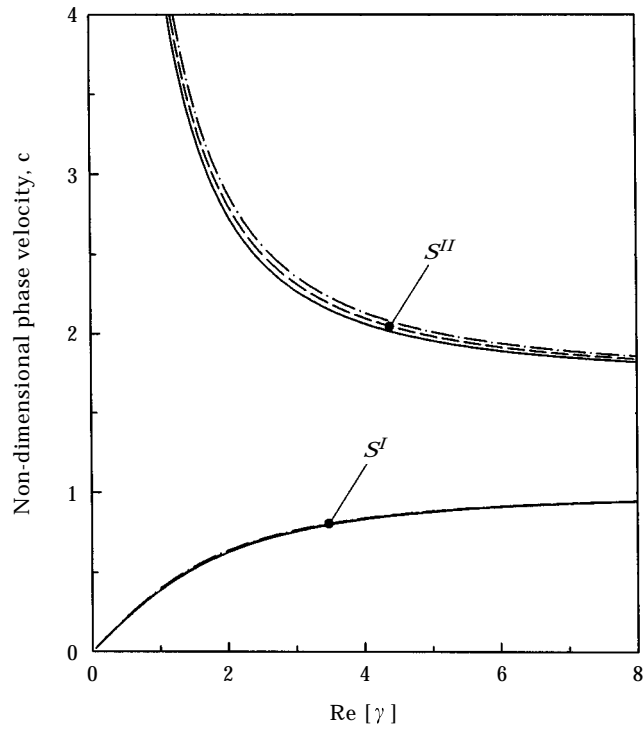


Figure 6. Non-dimensional phase velocity as a function of real wavenumber for three rotation speeds; $\alpha = 0.3378$, $\varepsilon = 0$; $\beta = 0$ (—), $\beta = 0.05$ (---), $\beta = 0.1$ (-.-).

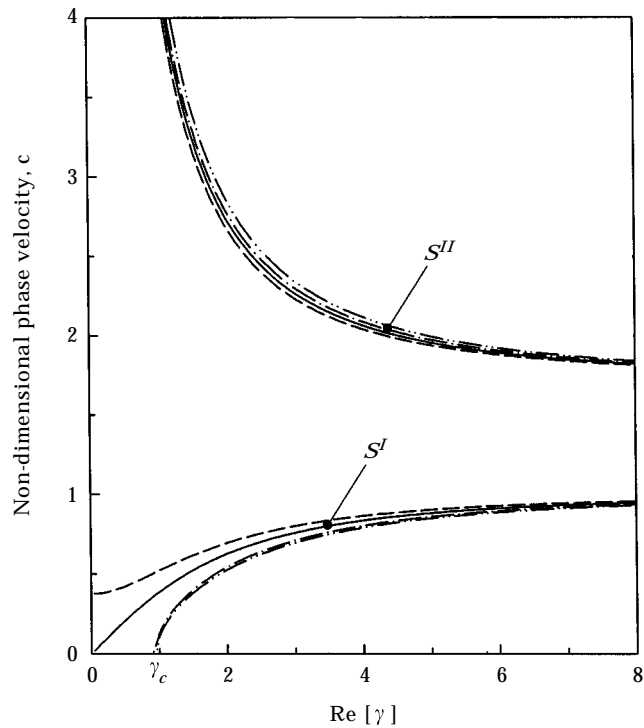


Figure 7. Non-dimensional phase velocity as a function of real wavenumber for three loading conditions; $\alpha = 0.3378$, $\beta = 0$; $\varepsilon = 0$ (—), $\varepsilon = 0.05$ (---), $\varepsilon = -0.05$ (-.-), $\varepsilon = -0.05$ with effects of axial deformation neglected (-.-.-).

Figure 6 shows the effects of the rotation speed on the phase velocity as a function of $\text{Re}[\gamma]$, i.e., for propagating waves. Note that only (positive) phase velocities for backward propagating waves are shown. Two distinct dispersion curves, approaching the asymptotic values of 1 and $1/\sqrt{\alpha}$, are seen in the figure. Moreover, the phase velocity of the S^I mode is upper bounded by the shear velocity, while the phase velocity of the S^{II} mode is lower bounded by the bar velocity. Again, the effects of the rotation speed are rather insignificant, especially for the S^I mode. For the S^{II} mode, the phase velocity increases with the rotation speed. However, the differences are small even at high rotation speed ($\beta = 0.05 \cong 44\,560$ r.p.m.).

Figure 7 shows the effects of the axial load on the phase velocities of propagating waves. It is seen that the axial load has significant influence on the phase velocities of S^I waves at low wavenumber (long wavelength), while its effects on S^{II} waves are relatively insignificant. Applying a compressive load decreases the phase velocities of S^I waves and increases those of S^{II} waves. A tensile load has the reverse effects. For S^I waves with wavenumber smaller than γ_c and under compressive loads, numerical results show that the phase velocities are positive imaginary. This implies that the wave amplitudes decay temporally. Under tensile loads, the phase velocities of S^I waves with long wavelength are relatively high (based on c_0 of 5200 m/s, the minimum phase velocity of the dashed curve in Figure 7 for S^I waves is about 1000 m/s which is about three times the speed of sound). In Figure 7, the dot-dot-dashed curves show the phase velocities of the waves under compressive loads and with the effects of the axial deformation neglected. These effects are rather insignificant for both modes.

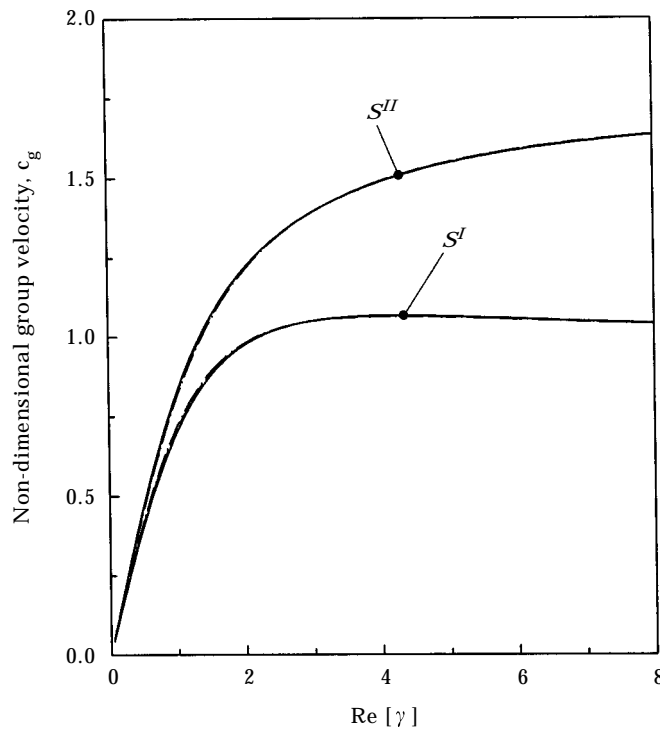


Figure 8. Non-dimensional group velocity as a function of real wavenumber for three rotation speeds; $\alpha = 0.3378$ and $\varepsilon = 0$; $\beta = 0$ (—), $\beta = 0.05$ (- - -), $\beta = 0.1$ (- · -).

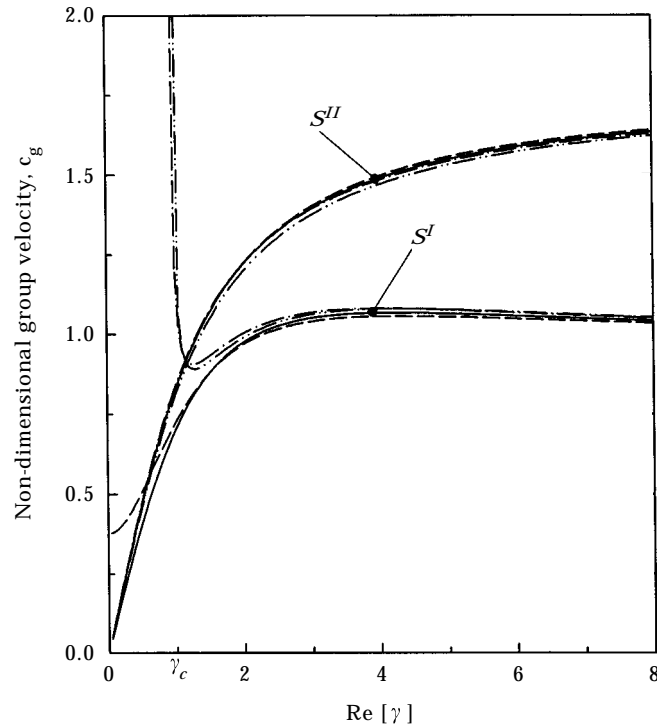


Figure 9. Non-dimensional group velocity as a function of real wavenumber for three loading conditions; $\alpha = 0.3378$ and $\beta = 0$; $\varepsilon = 0$ (—), $\varepsilon = -0.05$ (- - -), $\varepsilon = 0.05$ (- · - ·), $\varepsilon = -0.05$ with effects of axial deformation neglected (- · · -).

Another important property of waves propagating along a dispersive elastic waveguide is the group velocity c_g which is defined as the slope of the frequency spectrum

$$c_g = \frac{\partial \omega}{\partial \gamma}. \quad (18)$$

It is known that the group velocity and the phase velocity are equal only for waves propagating in non-dispersive media. The group velocity represents the aggregate behaviour of a number of waves travelling with different phase velocities. It can be shown from equation (15) that $\lim_{\gamma \rightarrow \infty} c_g = c_s$ for the S' mode and $\lim_{\gamma \rightarrow \infty} c_g = c_0$ for the S'' mode; the same asymptotic values as the phase velocity.

Figure 8 shows the effects of the rotation speed on the group velocities of propagating waves. As seen in the figure, the three curves in each mode are hardly distinguishable from each other. Hence, the rotation speed does not affect the group velocities of both S' and S'' modes. Figure 9 plots the group velocity as a function of real wavenumber (propagating waves) for three axial loads. It is noted that when the shaft model is under a compressive load, the group velocities of S' waves are infinite at γ_c and rapidly approach the asymptotic value of 1. Numerical results indicate that c_g is complex for $\gamma < \gamma_c$, implying that wave energy does not propagate at small wavenumbers since energy propagates at the group velocity [11–13]. When a tensile axial load is applied, the group velocities of S' waves are significantly higher at low wavenumbers; this has also been observed in Figure 7 for the case of the phase velocity. On the other hand, the effects of the axial load on S'' waves are insignificant. Moreover, contributions of the axial deformation are small for both S' and S'' waves. Comparing Figures 6 and 7 with 8 and 9, it is seen that the group velocities

of S' waves are always greater than the phase velocities, resulting in anomalous dispersion. However, the group velocities of S'' waves are always smaller than the phase velocities, resulting in normal dispersion.

5. SUMMARY AND CONCLUSIONS

The wave propagation in an infinitely long, rotating Timoshenko shaft subjected to an axial load is studied in this paper. The equations of motion are based on a finite strain theory including the contributions of the axial deformation to the transverse vibrations. Two cut-off frequencies corresponding to two frequency spectra are obtained. It is shown that the general wave solutions can be classified into four different cases (*Cases I–IV* as defined in equations (14a–d)). However, in engineering applications, *Case III* does not exist. The effects of the rotation speed and the axial load on the frequency spaces are examined. It is found that, in the presence of a compressive load and in the range of practical rotating speeds of the flexible shaft, the solutions of *Cases I* and *II* govern the wave motions in the shaft. The wave solution above the finite cut-off frequency is of *Case I*, while the wave solution below it is of *Case II* or *Case IV*.

The effects of the rotation speed and the axial load on the characteristics of wave propagation in the rotating Timoshenko beam are further examined in terms of the frequency spectra, phase velocity and group velocity. Some major conclusions are summarized as follows. (1) The rotation speed has no effect on the first frequency spectrum (S'). However, the rotation speed increases the frequencies in the second spectrum (S''). For a non-rotating shaft, the temporal response of attenuating waves is non-oscillatory beyond a certain $\text{Im}[\gamma]$. When the shaft is rotating, the temporal behaviour of these waves becomes oscillatory. (2) The effects of the axial load on both frequency spectra are stronger than those of the rotation speed. When the rotating shaft is compressed, there exists a critical real wavenumber (γ_c) below which no S' wave can propagate. It is also shown that the effects of axial deformation are insignificant for the S' spectrum, while frequencies are increased (over-predicted) for the S'' spectrum. Numerical results show that this over-prediction increases with the axial strain. (3) The rotation speed has almost no effect on both the phase velocity and the group velocity, except for a small increase in the phase velocity of the S'' waves. It is also shown that both the phase velocities and the group velocities of the two spectra have the same asymptotic behaviour and are bounded by the shear wave velocity and the wave velocity of a bar. (4) The effects of the axial load on both the phase velocity and the group velocity are similar. It is found that the axial load is important only for S' waves with long wavelength. In particular, a tensile load significantly increases the velocities. Under a compressive axial load, both the phase and group velocities are positive imaginary for real wavenumbers below γ_c , implying that the wave amplitudes decay temporally and that wave energy does not propagate.

ACKNOWLEDGMENTS

The authors wish to acknowledge the support of the National Science Foundation and the Institute of Manufacturing Research of Wayne State University for this research work.

REFERENCES

1. T. C. HUANG 1961 *ASME Journal of Applied Mechanics* **28**, 579–584. The effect of rotary inertia and of shear deformation on the frequency and normal mode equations of uniform beams with simple end conditions.

2. F. M. DIMENTBERG 1961 *Flexural Vibrations of Rotating Shafts*. London: Butterworth.
3. A. D. DIMAROGONAS and S. A. PAIPETIES 1983 *Analytical Method in Rotor Dynamics*. New York: Applied Science.
4. C. W. LEE 1993 *Vibration Analysis of Rotors*. Dordrecht, The Netherlands: Kluwer Academic Publishers.
5. S. H. CHOI, C. PIERRE and A. G. ULSOY 1992 *ASME Journal of Vibration and Acoustics* **114**, 249–259. Consistent modeling of rotating Timoshenko shafts subject to axial loads.
6. R. KATZ, C. W. LEE, A. G. ULSOY and R. A. SCOTT 1988 *Journal of Sound and Vibration* **122**, 131–148. The dynamic response of a rotating shaft subject to a moving load.
7. J. W. Z. ZU and R. P. S. HAN 1992 *ASME Journal of Applied Mechanics* **59**, 197–204. Natural frequencies and normal modes of a spinning Timoshenko beam with general boundary conditions.
8. C. A. TAN and W. KUANG 1995 *Journal of Sound and Vibration* **183**, 451–474. Vibration of a rotating discontinuous shaft by the distributed transfer function method.
9. B. A. H. ABBAS and J. THOMAS 1977 *Journal of Sound and Vibration* **51**, 123–137. The second frequency spectrum of Timoshenko beams.
10. G. R. BHASHYAM and G. PRATHAP 1981 *Journal of Sound and Vibration* **76**, 407–420. The second frequency spectrum of Timoshenko beams.
11. L. CREMER, M. HECKL and E. E. UNGAR 1973 *Structure-Borne Sound*. Berlin: Springer-Verlag.
12. K. F. GRAFF 1975 *Wave Motion in Elastic Solids*. Ohio State University Press.
13. F. FAHY 1985 *Sound and Structural Vibration* New York: Academic Press.
14. Y. K. LIN 1962 *International Journal of Mechanical Sciences* **4**, 409–423. Free vibrations of a continuous beam on elastic supports.
15. D. J. MEAD 1994 *Journal of Sound and Vibration* **171**, 695–702. Waves and modes in finite beams: application of the phase-closure principle.
16. B. R. MACE 1984 *Journal of Sound and Vibration* **97**, 237–246. Wave reflection and transmission in beams.
17. A. ARGENTO and R. A. SCOTT 1995 *Wave Motion* **21**, 67–74. Elastic wave propagation in a Timoshenko beam spinning about its longitudinal axis.
18. C. A. TAN and B. KANG 1998 *Journal of Sound and Vibration* **213**, 483–510. Wave reflection and transmission in an axially strained, rotating Timoshenko shaft.